Optica Applicata, Vol. LV, No. 3, 2025
DOI: 10.37190/oa/207948

Fano resonance in a MIM waveguide structure with chiral gammadion resonance cavity

Taiming Sun*, Nianshun Zhao, Zheng Li, Yunyan Zhou, Kang Fu

School of Mechanical and Electrical Engineering, HuangShan University, Anhui, 245041, China

*Corresponding author: stm314159@sina.com

A compact plasmonic nanosensor has been described, which consists of a metal–insulator–metal (MIM) waveguide and two symmetric rectangular stubs coupled with a gammadion resonance cavity (GRC) with chiral properties. The transmission characteristics and magnetic field distribution of the MIM waveguide structure are simulated by employing the finite element method (FEM). Results revealed that a Fano resonance is excited in the designed whole waveguide system. The Fano resonance can be tuned by the structural parameters of the waveguide system. The MIM waveguide structure with optimized parameters can be applied in identify different concentrations of glucose solution. The sensitivity achieves up to 945 nm/RIU. This proposed structure has potential applications in the biosensors and optical communications.

Keywords: Fano resonance, metal–insulator–metal (MIM) waveguide structure, gammadion resonance cavity (GRC), finite element method (FEM), full width at half maximum (FWHM).

1. Introduction

Surface plasmons (SPs), which are formed by the interaction between the incident photons and freely oscillating electrons on the surface of the metal, are the electromagnetic waves propagating along the metal surface [1,2]. SPs include surface plasmon polaritons (SPPs) and localized surface plasmons (LSP), which can break the diffraction limit and excite high intensity near-fields [3,4]. Among all waveguide structures, the metal–insulator–metal (MIM) waveguide structures have advantages including low band loss, low fabrication cost, easiness to integrate, and stronger restraint of SPs [5-8]. Therefore, large amounts of optical devices based on MIM waveguide structure have been proposed, such as biosensors, switches, filters, and couplers [9-12].

Peculiar optical properties have been found in the MIM waveguide system. Fano resonance is a resonance phenomenon that produces a sharp and asymmetric spectral narrow line-shape, owing to which, the transmission spectrum of the Fano structure exhibits a relatively narrow full width at half maximum (FWHM) [13,14]. It originates from the mutual coupling between broad continuum state and narrow discrete state of

EM modes [15,16]. Fano resonance forming in MIM waveguide system is extremely sensitive to the refractive index of medium environment and structural parameters, which is usually designed as nanosensors [17]. At present, large numbers of nanosensors based on the Fano resonance of MIM waveguide system have been reported in nanophotonics. ZHU *et al*. presented a plasmon waveguide structure consisting of a MIM waveguide and a semicircular resonant cavity coupled with a key-shaped resonant cavity, which can attain a sensitivity of 1261.67 nm/RIU [9]. QIAO *et al*. proposed a plasmonic nanosensor composed of a baffle and an M-type cavity with a sensitivity of 780 nm/RIU [18]. ZHAO *et al*. introduced a nanosensor based on MIM waveguide structure, that consisted of two silver baffles coupled with a ring cavity. The sensitivity of this nanosensor reached 718 nm/RIU [19]. In these studies, these structures are too complex to integrate, and the sensitivity is relatively low. Moreover, chiral nanostructure have become a growing interest in SPs optics owing to its marvellous optical properties such as circular dichroism, negative refractive index, and optical rotation [20-22]. However, to date, there are few studies paying attention to the sensing characteristics and Fano resonance of MIM waveguide with chiral structure. Therefore, it is crucial to develop a compact MIM waveguide system with chiral structure and remarkable sensitivity in sensing.

In this paper, we propose a compact MIM waveguide structure, which consists of a MIM waveguide and two symmetric rectangular stubs coupled with a gammadion resonance cavity (GRC) with chiral properties. The transmission spectrum and magnetic field distribution of the MIM waveguide structure are simulated by employing the finite element method (FEM). Then, the Fano resonance is obtained in the designed whole waveguide system. The effect of structural parameters of the waveguide system such as the height and length of rectangular arms, the height and width of two symmetric rectangular stubs, and the coupling distances of GRC and two symmetric rectangular stubs on Fano resonance are analyzed. Finally, the sensing characteristics of the MIM waveguide structure with optimized parameters is investigated. This study mainly focus on the theoretical exploration of the Fano resonance of MIM waveguide structure with chiral gammadion resonance cavity, with subsequent application of the optimized structural in the field of nanosensor.

2. Structure model and analytical method

To study the Fano resonance of MIM waveguide with chiral structure, the MIM waveguide structure comprising the MIM waveguide with the GRC coupled with two symmetric rectangular stubs is proposed. Figure 1 shows the schematic diagram of the constructed waveguide structure. The white area represents air and the gray area represents metallic silver. The GRC can be seen as consisting of a cross and four rectangular arms. The length and width of the rectangular arm of GRC are defined as L and w_1, respectively; w_2 and H represent the width and height of the two symmetric rectangular stubs, respectively. The coupling distance between the GRC and the two symmetric rectangular stubs is denoted as G.

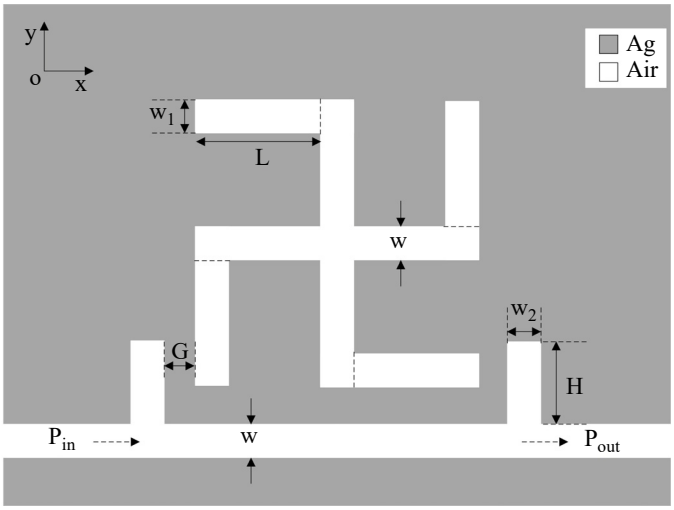

Fig. 1. Schematic diagram of the MIM waveguide structure with two symmetric rectangular stubs coupled with a gammadion resonance cavity (GRC).

Finite element method (FEM) is employed to calculate the light propagation through the MIM waveguide structure. Since the thickness of the proposed structure was significantly longer than the light wavelength, the 2D model can be used to approximate the 3D model for simulation calculations. The dielectric constant of metallic silver is obtained using the Drude model [23]:

$$\varepsilon_{\mathrm{m}}(\omega) = \varepsilon_{\infty} - \frac{\omega_{\mathrm{p}}^2}{\omega(\omega + j\gamma)} \tag{1}$$

where ω is the angular frequency of the incident wave, $\varepsilon_{\infty} = 3.7$ represents dielectric constant at infinite angular frequency, $\omega_{\mathrm{p}} = 9.1$ eV is the plasmon frequency of the metallic silver, $\gamma = 0.018$ eV is the electron collision frequency. The transmission spectrum of the compact waveguide system was expressed by $T = P_{\mathrm{out}}/P_{\mathrm{in}}$, where $P_{\mathrm{in(out)}}$ is the power flux input (output) of the waveguide system.

3. Results and discussion

3.1. Transmittance characteristic analysis

To clearly understand the transmission characteristics of the MIM waveguide system with GRC, we calculated the transmission spectrum of the designed waveguide structure, the structural parameters were set as follows: $w = w_1 = w_2 = 50$ nm, $L = 175$ nm, $H = 70$ nm, and $G = 10$ nm. Figure 2 shows the transmission spectra of single GRC, single two symmetric rectangular stubs and the entire structure. The transmission spectra of single two symmetric rectangular stubs have high and stable transmittance in the range of 900 to 1400 nm. It can be regarded as broad continuous state. Meanwhile,

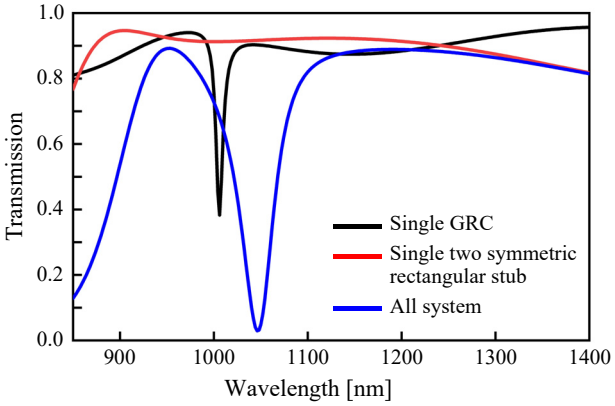

Fig. 2. Transmission spectra of the single two symmetric rectangular stubs (red line), the single GRC (black line), and the whole system (blue line).

a transmission dip is observed for single GRC at 1006 nm, which can be considered as a narrow discrete state. In the transmission spectra of the whole waveguide system as shown in the blue line, a sharp and asymmetric Fano line-shape is observed as a result of the mutual coupling between the GRC and two symmetric rectangular stubs. This phenomenon originates from the coherent superposition between broad continuous state and narrow discrete state [15].

To understand the internal mechanism of Fano resonance of the proposed structure more clearly, the distribution of H_z field in the whole system at the resonance peak ($\lambda = 952$ nm) and the resonance dip ($\lambda = 1046$ nm) are displayed in Fig. 3. From Fig. 3(b), it can be observed that the strong H_z field is confined in the GRC and the left side of the symmetrical rectangular stub, which result in the SPPs cannot transmit through the waveguide. In Fig. 3(a), it can be seen that the relatively strong H_z field distribution was in the GRC and the two symmetrical rectangular walls. Obviously, due to the coupling of the H_z field in the GRC and two symmetric rectangular stubs,

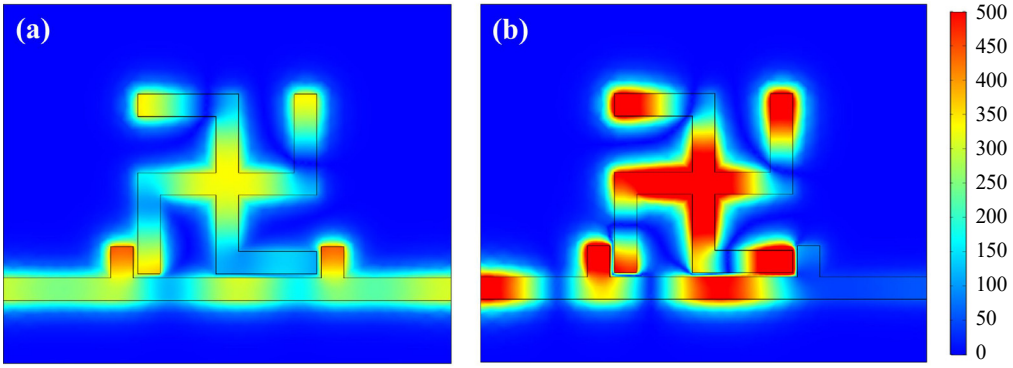

Fig. 3. The H_z field distribution of the whole system at (a) the resonance peak ($\lambda = 952$ nm), and (b) the resonance dip ($\lambda = 1046$ nm).

the strong H_z is excited in the waveguide and the SPPs can pass through the waveguide structure.

3.2. Influence of structural parameters on Fano resonance

The gammadion-shaped structure has marvellous optical properties because of its rectangular arm. We then studied the influence of geometrical parameters of the rectangular arm on the Fano resonance. Figure 4(a) presents the transmission spectrum of the waveguide structures with different rectangular arm lengths, where the rectangular arm length L increases from 135 to 195 nm. Here other parameters are fixed at $w_1 = w_2 = 50$ nm, $H = 100$ nm, and $G = 10$ nm. Figure 4(b) illustrates the FWHM line graphs for the peak and the dip of Fano resonance. It is seen in Fig. 4(a) that as the length L increases, the Fano resonance exhibits a significant red shift. The transmittance of the peak increases from 0.56 to 0.87, and the dip has been basically unchanged. Obviously, the length of the rectangular arm L has great influence on the resonance wavelength and peak value of Fano resonance. As shown in Fig. 4(b), it was found that as the length L increases, the FWHM of peak (F_p) indicates an upward trend, and the FWHM of dip (F_d) shows a general downward trend. In view of both the line graphs, it can be observed that the average value of F_p and F_d is the lowest when $L = 155$ nm. Therefore, this value is considered to be the optimal value, we choose to use a rectangular arm of 155 nm.

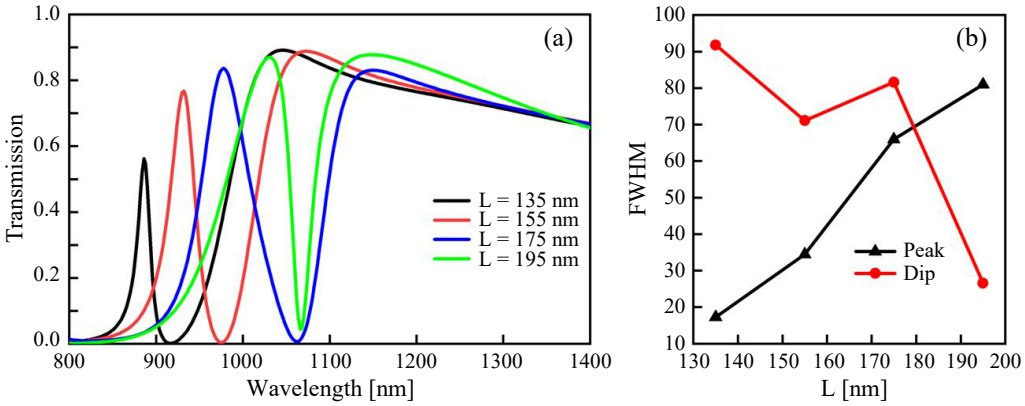

Fig. 4. (a) The transmittance spectra of the GRC as the length of rectangular arm L increases from 135 to 195 nm. (b) The change curves of FWHM for the peak and the dip of Fano resonance.

In addition, we investigate the influence of the rectangular arm width on the Fano resonance. Figure 5(a) shows the transmission spectra when the width of rectangular arm of GRC, w_1, increases from 50 to 110 nm. The other parameters were fixed as $w_2 = 50$ nm, $L = 155$ nm, $H = 100$ nm, and $G = 10$ nm. It can be observed from Fig. 5(a) that as the rectangular arm width w_1 increases, the Fano resonance shows a clear blue shift, and the transmission peaks decrease from 0.77 to 0.12. These indicate that the

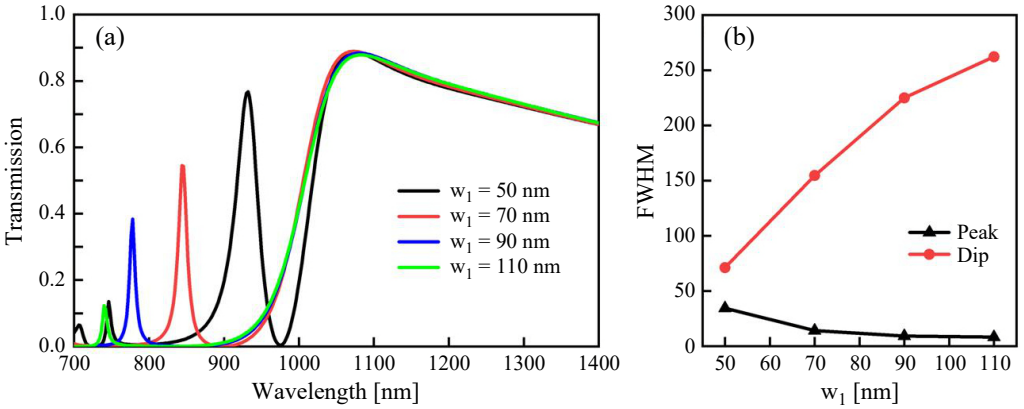

Fig. 5. (a) The transmittance spectra of the GRC as the width of rectangular arm w_1 increases from 50 to 110 nm. (b) The change curves of FWHM for the peak and the dip of Fano resonance.

intensity and resonance wavelength of Fano resonance was affected by the width of rectangular arm of GRC. Figure 5(b) shows the FWHM of the peak and the dip with different rectangular arm widths. Obviously, it can be seen that with the change of the rectangular arm width, the F_p is basically unchanged, whereas the F_d increases sharply. Based on the changing trend of FWHM in Fig. 5(b), we choose the rectangular arm width w_1 = 50 nm as the optimal value.

The rectangular arm and two symmetric rectangular stubs exhibit strong coupling interaction, so the influence of the width w_2 and height H of the two symmetric rectangular stubs and the coupling distance G on Fano resonance was then examined, respectively. Figure 6(a) displays the transmission spectra changes as the height H increases from 60 to 120 nm. Here the other parameters are fixed as $w_1 = w_2 = 50$ nm, $L = 155$ nm, and $G = 10$ nm. As shown in Fig. 6(a), the Fano resonance exhibit a red

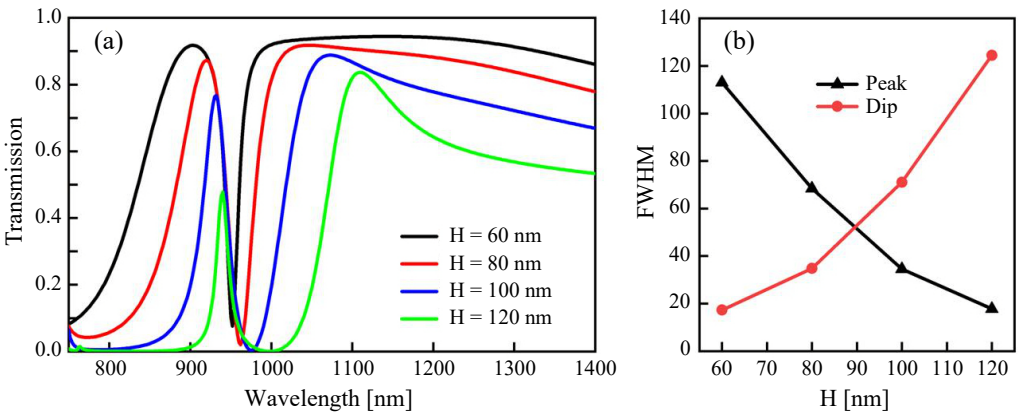

Fig. 6. (a) The transmittance spectra of the two symmetric rectangular stubs as its height H increases from 60 to 120 nm. (b) The change curves of FWHM for the peak and the dip of Fano resonance.

shift as H increases. Moreover, the transmittance of the peak decreases significantly from 0.92 to 0.48. These analyses indicate that the peak value of Fano resonance was affected by the height of two symmetric rectangular stubs. And as shown in Fig. 6(b), with the increases of height H of two symmetric rectangular stubs, the curves of F_p and F_d demonstrate a decreasing trend and an increasing trend, respectively, intersecting at H = 90 nm. Based on the variation characteristics of the F_p and F_d in Fig. 6(b), we choose to use the symmetric rectangular stub height H of 90 nm.

Figure 7(a) shows the transmission spectra of the waveguide structures with different symmetric rectangular stubs width w_2, where the width changes from 70 to 130 nm with an interval of 20 nm. The other structural parameters are: w_1 = 50 nm, L = 155 nm, H = 90 nm, and G = 10 nm. As shown in Fig. 7(a), the wavelength of Fano resonance is unchanged as w_2 increases. The transmittance of the peak decreases from 0.79 to 0.50, and the transmittance of the dip indicates only a minimal change, increasing from 0.0103 to 0.0113. This means that the resonance wavelength of the Fano resonance is not influenced by the width of two symmetric rectangular stubs. Figure 7(b) displays the FWHM of the peak and dip. As w_2 increases, the curves of F_p demonstrate a decreasing trend slowly, whereas the F_d presents an increasing trend markedly. Based on the change trend of FWHM in Fig. 7(b), we chose to use the w_2 of 70 nm to build the prototype plasmonic nanosensor.

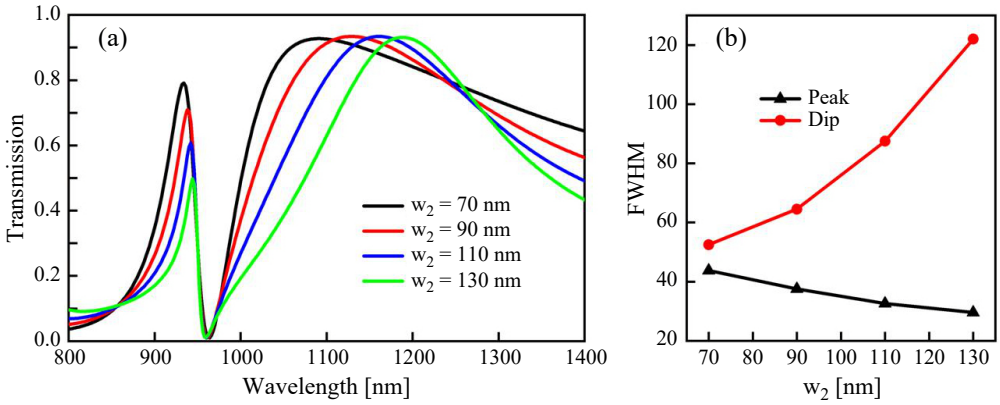

Fig. 7. (a) The transmittance spectra of the two symmetric rectangular stubs as its width w_2 increases from 70 to 130 nm. (b) The change curves of FWHM for the peak and the dip of Fano resonance.

Based on the above optimized parameters, the influence of the coupling distance G between two symmetric rectangular stubs and GRC on Fano resonance was studied.

Figure 8(a) presents the transmission spectra when the coupling distance G increases from 10 to 15 nm. The other structural parameters were as follows: w_1 = 50 nm, w_2 = 70 nm, L = 155 nm, and H = 90 nm. As shown in Figure 8(a), when G increases, the Fano resonance manifests a slightly blue shift. The transmittance of the peak decreases from 0.79 to 0.39, while the transmittance of the dip increases from 0.01 to 0.05. Obviously, the intensity of Fano resonance is gradually weakening as G increases.

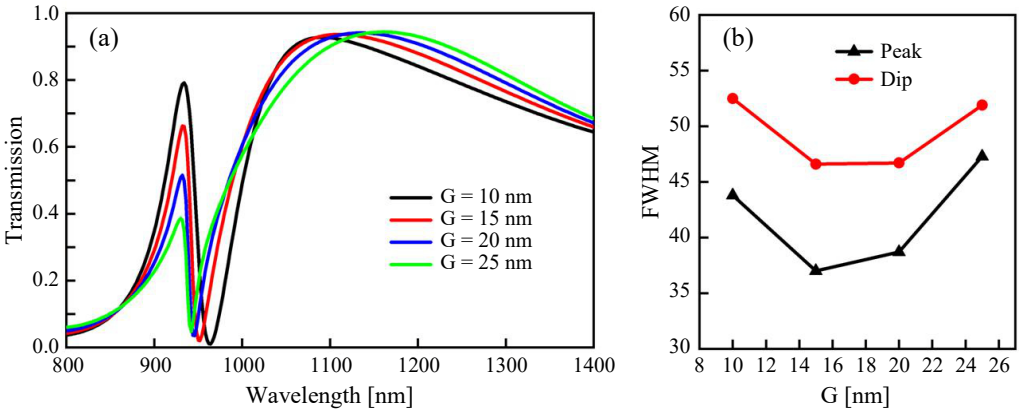

Fig. 8. (a) The transmittance spectra of the GRC coupled to the two symmetric rectangular stubs with different coupling distances G. (b) The change curves of FWHM for the peak and the dip of Fano resonance.

The corresponding FWHM of the peak and dip are presented in Fig. 8(b). As the coupling distance G increases, the change curves of F_p and F_d present a parabola line, and the lowest point is at G = 15 nm. Therefore, we use the coupling distance G = 15 nm as the standard value.

3.3. Concentration of glucose solution identification

In view of the conclusions that the Fano resonance is influenced by structural parameters of the MIM waveguide structure comprising the MIM waveguide with the GRC coupled with two symmetric rectangular stubs, the application of the MIM waveguide structure with optimized parameters in the field of nanosensor is explored. We simulated the transmission spectrum in different concentrations of glucose solution. The average

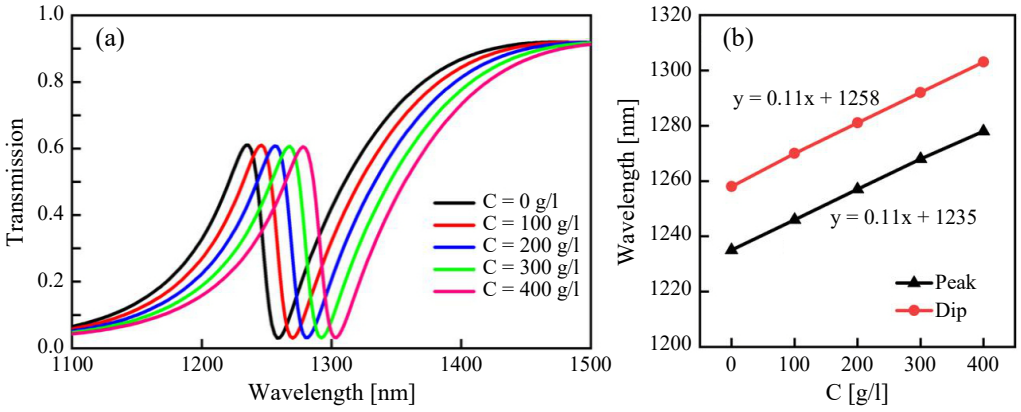

Fig. 9. (a) The transmittance spectra of the MIM waveguide structure with optimized parameters when the glucose concentration C increases from 0 to 400 g/l. (b) The relationship between the wavelength of peak and dip of Fano resonance and the glucose concentration C.

refractive index of glucose solution with different concentrations of glucose is described as [24]:

$$n_{gs} = 0.00011889\,C + 1.33230545 \tag{2}$$

where C is glucose concentration (g/l) and n_{gs} is the average refractive index of glucose solution. Figure 9(a) shows the transmittance spectra of glucose solution with the concentration C ranging from 0 to 400 g/l. It was found from Fig. 9(a) that as the glucose concentration increased, the Fano resonance exhibited a clearly red shift, whereas the transmittance of dip and peak remained basically unchanged. Specifically, the wavelength of the peak increases from 1235 to 1278 nm and the wavelength of dip increases from 1258 to 1303 nm. More importantly, the wavelength of peak and dip varies linearly with the glucose concentration C as shown in Fig. 9(b).

Generally, the crucial indicator for assessing sensors is sensitivity S. Moreover, the sensitivity S is defined as [25]:

$$S = \Delta\lambda/\Delta n \quad \text{[nm/RIU]} \tag{3}$$

where the wavelength shift of Fano resonance is expressed by $\Delta\lambda$ and the change of refractive index is described by Δn. Based on Eq. (3), the sensitivity S at the dip is 945 nm/RIU.

The sensitivity S of the proposed plasmonic nanosensor is compared with other sensor structures in Table 1. Obviously, compared with previous results [18,19,26,27], where the sensitivity S was 780, 718, 753 and 600 nm/RIU, the sensitivity S of our work was higher. Meanwhile, compared to Fano system [9], although the sensitivity S is higher than our work, the structure is too complex to integrate.

T a b l e 1. Comparison of the sensitivity with references.

Reference	Sensitivity [nm/RIU]
[9]	1261.67
[18]	780
[19]	718
[26]	753
[27]	600
This work	945

4. Conclusions

In summary, this study presents a compact plasmonic nanosensor, which consists of a MIM waveguide and two symmetric rectangular stubs coupled with a GRC. The Fano resonance is excited in the designed whole waveguide system and can be tuned by the structural parameters of the waveguide system. Specially, the resonance wavelength of the Fano resonance is mainly adjusted by the width and length of the rectangular arm in the GRC. Based on the excellent sensing characteristics of Fano resonance struc-

ture, the MIM waveguide structure with optimized parameters is applied in identify different concentrations of glucose solution. The sensitivity achieves up to 945 nm/RIU. Moreover, the designed waveguide system can also be applied in the sensing of other liquids. This study provides a helpful direction for designing plasmonic nanosensor, and expand the application of nanophotonic devices in biosensors and optical communications.

Acknowledgment
This work was supported by the Natural Science Foundation for Higher Education Institutions of Anhui Province (grant no. KJHS2021B10) and the Major Project of Natural Science Foundation for Anhui Provincial Education Department (grant no. 2022AH040270).

Conflict of interest
The authors declare that they have no known competing financial interests or personal relationships that could have appeared to influence the work reported in this paper.

References

[1] BARNES W.L., DEREUX A., EBBESEN T.W., *Surface plasmon subwavelength optics*, Nature **424**(6950), 2003: 824-830. https://doi.org/10.1038/nature01937
[2] JANKOVIC N., CSELYUSZKA N., *Multiple Fano-like MIM plasmonic structure based on triangular resonator for refractive index sensing*, Sensors **18**(1), 2018: 287. https://doi.org/10.3390/s18010287
[3] LIN L., ROBERTS A., *Light transmission through nanostructured metallic films: Coupling between surface waves and localized resonances*, Optics Express **19**(3), 2011: 2626-2633. https://doi.org/10.1364/oe.19.002626
[4] GRAMOTNEV D.K., BOZHEVOLNYI S.I., *Plasmonics beyond the diffraction limit*, Nature Photonics **4**(2), 2010: 83-91. https://doi.org/10.1038/nphoton.2009.282
[5] LU Q., CHEN D., WU G., *Low-loss hybrid plasmonic waveguide based on metal ridge and semiconductor nanowire*, Optics Communications **289**, 2013: 64-68. https://doi.org/10.1016/j.optcom.2012.09.077
[6] RAHAD R., ALI A., PIAS M.K.H., FARABI M., ISLAM M.A., FAHIM A.A., *Plasmonic metal-insulator-metal (MIM) refractive index sensor for glucose level monitoring*, Plasmonics **19**(5) 2024: 2605-2614. https://doi.org/10.1007/s11468-024-02201-y
[7] FANG Y., SUN M., *Nanoplasmonic waveguides: Towards applications in integrated nanophotonic circuits*, Light: Science & Applications **4**, 2015: e294. https://doi.org/10.1038/lsa.2015.67
[8] TAO J., HUANG X.G., LIN X., ZHANG Q., JIN X., *A narrow-band subwavelength plasmonic waveguide filter with asymmetrical multiple-teeth-shaped structure*, Optics Express **17**(16), 2009: 13989-13994. https://doi.org/10.1364/oe.17.013989
[9] ZHU J., LI N., *MIM waveguide structure consisting of a semicircular resonant cavity coupled with a key-shaped resonant cavity*, Optics Express **28**(14), 2020: 19978-19987. https://doi.org/10.1364/oe.395696
[10] PENG R., WANG S., ZHANG Z., YANG X., *Surface plasmon filter based on metal-insulator-metal waveguide with multi-stopband and high filtering efficiency*, Plasmonics **19**(4), 2024: 1977-1988. https://doi.org/10.1007/s11468-023-02112-4
[11] YAN Z., YAN S., XU Z., CHEN C., CAO Y., YAN X., WANG C., WU T., *Multi-structure-based refractive index sensor and its application in temperature sensing*, Sensors **25**(2) 2025: 412. https://doi.org/10.3390/s25020412
[12] ZUN J., WU Z., FU D., LU G., HU H., *Novel optical switch and four-to-one data selector utilizing an MIM waveguide structure based on surface plasmon polaritons*, Measurement **241**, 2025: 115681. https://doi.org/10.1016/j.measurement.2024.115681

[13] Fano U., *Effects of configuration interaction on intensities and phase shifts*, Physical Review **124**(6), 1961: 1866-1878. https://doi.org/10.1103/physrev.124.1866

[14] Yang X., Hua E., Wang M., Wang Y., Wen F., Yan S., *Fano resonance in a MIM waveguide with two triangle stubs coupled with a split-ring nanocavity for sensing application*, Sensors **19**(22), 2019: 4972. https://doi.org/10.3390/s19224972

[15] El Haffar R., Farkhsi A., Mahboub O., *Optical properties of MIM plasmonic waveguide with an elliptical cavity resonator*, Applied Physics A **126**, 2020: 486. https://doi.org/10.1007/s00339-020-03660-w

[16] Lovera A., Gallinet B., Nordlander P., Martin O.J.F., *Mechanisms of Fano resonances in coupled plasmonic systems*, ACS Nano **7**(5), 2013: 4527-4536. https://doi.org/10.1021/nn401175j

[17] Chen J., Li J., Liu X., Rohimah S., Tian H., Qi D., *Fano resonance in a MIM waveguide with double symmetric rectangular stubs and its sensing characteristics*, Optics Communications **482**, 2021: 126563. https://doi.org/10.1016/j.optcom.2020.126563

[18] Qiao L., Zhang G., Wang Z., Fan G., Yan Y., *Study on the Fano resonance of coupling M-type cavity based on surface plasmon polaritons*, Optics Communications **433**, 2019: 144-149. https://doi.org/10.1016/j.optcom.2018.09.055

[19] Zhao X., Zhang Z., Yan S., *Tunable Fano resonance in asymmetric MIM waveguide structure*, Sensors **17**(7), 2017: 1494. https://doi.org/10.3390/s17071494

[20] Bai B., Laukkanen J., Lehmuskero A., Turunen J., *Simultaneously enhanced transmission and artificial optical activity in gold film perforated with chiral hole array*, Physical Review B **81**(11), 2010: 115424. https://doi.org/10.1103/PhysRevB.81.115424

[21] Arteaga O., Sancho-Parramon J., Nichols S., Maoz B.M., Canillas A., Bosch S., Markovich G., Kahr B., *Relation between 2D/3D chirality and the appearance of chiroptical effects in real nanostructures*, Optics Express **24**(3), 2016: 2242-2252. https://doi.org/10.1364/oe.24.002242

[22] Alali F., Kim Y.H., Baev A., Furlani E.P., *Plasmon-enhanced metasurfaces for controlling optical polarization*, ACS Photonics **1**(6), 2014: 507-515. https://doi.org/10.1021/ph5000192

[23] Han Z., Bozhevolnyi S.I., *Plasmon-induced transparency with detuned ultracompact Fabry-Perot resonators in integrated plasmonic devices*, Optics Express **19**(4), 2011: 3251-3257. https://doi.org/10.1364/oe.19.003251

[24] Yeh Y.-L., *Real-time measurement of glucose concentration and average refractive index using a laser interferometer*, Optics and Lasers in Engineering **46**(9), 2008: 666-670. https://doi.org/10.1016/j.optlaseng.2008.04.008

[25] Shen S., She S., Wang Z., Tan Q., Xiong J., Zhang W., *MIM waveguide structure consisting of two triangle stubs, side-coupled with an eight-like resonant cavity*, Optics Communications **495**, 2021: 127087. https://doi.org/10.1016/j.optcom.2021.127087

[26] Li X., Zhang Z., Guo F., Huang Y., Zhang B., Zhang L., Yang Q., Tan Y., Liu X., Bai H., Song Y., *Tunable plasmonically induced reflection in HRR-coupled MIM waveguide structure*, Optik **199**, 2019: 163353. https://doi.org/10.1016/j.ijleo.2019.163353

[27] Li S., Zhang Y., Song X., Wang Y., Yu L., *Tunable triple Fano resonances based on multimode interference in coupled plasmonic resonator system*, Optics Express **24**(14), 2016: 15351-15361. https://doi.org/10.1364/oe.24.015351

Received April 9, 2025
in revised form June 29, 2025